Supporting Information

Bidirectional Electronic Modulation between Active Site and Support for Synergistically Enhanced Alkaline Hydrogen Evolution

Haijun Wang,[a] Jiatong Wang,[a] Ruonan Wang*[b] and Bohua Dong*[a]

[a] School of Materials Science and Engineering, Ocean University of China, 1299 Sansha Road, Qingdao, Shandong Province, 266404, P. R. China. E-mail: dongbohua@ouc.edu.cn

[b] School of Department of Mechanical and Electrical Engineering, Jining Polytechnic, Jining 272000, Shandong, China. E-mail: WRN2024@163.com

*Corresponding author

E-mail address: dongbohua@ouc.edu.cn

Chemicals.

Zirconium(Ⅳ) oxynitrate hydrate ($ZrO(NO_3)_2 \cdot xH_2O$, AR 99.5%), Ruthenium chloride ($RuCl_3 \cdot xH_2O$, 35.0-42.0%), Chloroplatinic acid hydrate ($H_2PtCl_6 \cdot xH_2O$, ≥99.9%), Potassium phosphate monobasic (KH_2PO_4, AR, 99.5%) and potassium phosphate dibasic ($K_2HPO_4 \cdot 3H_2O$, AR, 99.0%) were purchased from Aladdin Reagent Co., Ltd. Commercial Pt/C (20%) was obtained from Johnson-Matthey Corp. Nafion (5 wt.%) was supplied by Alfa Aesar, Methanol (CH_3OH, AR, ≥99.5%) and ethanol (CH_3CH_2OH, AR, ≥99.7%) were purchased from Tianjin Fuyu Fine Chemical Co., Ltd., and Phosphoric acid (H_3PO_4, AR ≥85%) was purchased from Sinopharm Chemical Reagent Co., Ltd. The HCP331N carbon cloth was procured from Suzhou Sinero Technology Co., Ltd. All reagents were utilized in received condition without any additional purification. Ultrapure water (deionized) was used in all the experiments.

Synthesis of ZrP

ZrP was synthesized following the methods described in the previously reported literature.1 Firstly, 1 mmol of $ZrO(NO_3)_2 \cdot xH_2O$ was dissolved in 25 mL of 6 M H_3PO_4 under continuous heating and stirring at 60 °C in a water bath until complete dissolution was achieved. The resulting solution was then transferred into a 50 mL Teflon-lined stainless-steel autoclave and heated at 200 °C for 24 hours. After the reaction, the system was naturally cooled to room temperature, and the product was collected via centrifugation. The precipitate was thoroughly washed multiple times with a mixture of ethanol and deionized water, then redispersed in 10 mL of deionized water for further use.

Synthesis of ZrP/Pt

Firstly, dissolve 3.2 mg of $H_2PtCl_6 \cdot xH_2O$ in 0.5 mL of deionized water to prepare the Pt precursor solution. Subsequently, transfer this solution into a 50 mL beaker containing 28 mL of methanol, followed by the addition of 2.5 mL of ZrP dispersion and 9 mL of deionized water. The resulting mixture is then subjected to ultrasonic treatment for 15 minutes, after which nitrogen gas is purged through the solution for 20 minutes. Following degassing, the mixture is stirred under ultraviolet irradiation for 1 hour. After completion of the reaction, the product is collected via centrifugation, washed repeatedly with ethanol, and finally dried overnight in a vacuum oven at 60 °C. (The quantities of chloroplatinic acid employed in samples ZrP/0.5Pt and ZrP/1.5Pt were 1.6 mg and 4.8 mg, respectively).

Materials characterization

X-ray diffraction (XRD) patterns were obtained using a Bruker D8 Advance X-ray diffractometer with Cu Kα radiation, scanning from 10° to 70° at a rate of 5° per minute. SEM was conducted on GeminiSEM 300, ZEISS. TEM and High-resolution TEM (HRTEM) were conducted on Thermofisher Talos F200x at the voltage of 200 kV. High-angle annular dark-field scanning transmission electron microscopy (HAADF-STEM) and HAADF-STEM energy dispersive X-ray spectroscopy (HAADF-STEM-EDX) were conducted on Thermo Themis Z at the voltage of 200 kV. X-ray photoelectron spectroscopy (XPS) measurements were performed on a Thermo Scientific K-Alpha X-ray photoelectron spectrometer with an Al excitation source. The elemental composition was determined using inductively coupled plasma mass spectrometry (ICP-OES, Agilent 5110). For ICP analysis, the sample digestion procedure was as follows: the samples were digested using 10 mL of aqua regia (a mixture of concentrated nitric acid and hydrochloric acid in a 1:3 volume ratio). The digestion was performed in a microwave digestion system under controlled temperature and pressure to ensure complete dissolution of the samples. After digestion, the solution was diluted with deionized water to a total volume of 5 mL to ensure a concentration suitable for ICP-OES analysis, allowing for accurate determination of the Pt and Ru content. The insitu Raman tests were conducted using an in-situ electrochemical Raman cell (Model: EC-RAIR-H), manufactured by Beijing Scistar Technology Co., Ltd. The cell was operated using a CHI 660E electrochemical workstation (Shanghai Chenhua, China). The in situ Raman spectra were collected using a Raman spectroscope (Invia Qontor) at a wavelength of 532 nm.

Electrochemical measurements

All electrochemical measurements were conducted using a CHI 660E electrochemical workstation (Shanghai Chenhua, China) in a standard three-electrode cell configuration with 1.0 MKOH as the electrolyte. The pH was verified and recorded immediately after preparation to ensure consistency for

subsequent data analysis. Additionally, prior to each cathodic linear sweep voltammetry (LSV) measurement for the hydrogen evolution reaction (HER), the 1 M KOH solution was purged with high-purity hydrogen gas for at least 30 minutes to ensure complete saturation. The hydrogen gas was supplied by a hydrogen generator (Model: CEH300; Beijing China Education Au-light Co., Ltd.). A Platinum sheet electrode and Hg/HgO electrode were employed as the counter electrode (CE) and reference electrode (RE), respectively. All potentials were referenced to the reversible hydrogen electrode (RHE) and converted according to the Nernst equation: $E_{RHE} = E_{Hg/HgO} + 0.098\ V + 0.0591 \times pH$. The as-synthesized ZrP/Pt electrocatalyst (1.8 mg) and 1 mg of carbon (Ketjen Black-300) were uniformly dispersed in a mixture consisting of 970 µL of ethanol and 30 µL of Nafion solution. After sonication for 1 h, 250 µL of homogeneous ink was deposited onto a carbon cloth electrode (1×1.5 cm^2) and allowed to dry completely under ambient conditions at room temperature. The total loading of active materials (catalyst and carbon black) on the surface of the carbon cloth substrate was 700 µg cm^{-2}. The 20% Pt/C electrocatalysts sample (1.8 mg) was dispersed in a solvent mixture consisting of 970 µL of ethanol and 30 µL of Nafion solution. Following ultrasonication for 1 hour to ensure homogeneity, 250 µL of the resulting uniform ink was deposited onto a carbon cloth electrode (area: 1×1.5 cm^2) and allowed to dry completely under ambient conditions at room temperature. The Pt loading on the prepared 20% Pt/C electrode was 100 µg cm^{-2}. Before the HER measurements, cyclic voltammetry (CV) was carried out in a potential range of 0 to -0.5 V (vs. RHE) in 1 M KOH at a scan rate of 100 mV s^{-1}, with each CV test consisting of 50 cycles. A preconditioning protocol involving at least 20 CV cycles was performed to ensure electrochemical stability and achieve a reproducible current response. Polarization curves were obtained via linear sweep voltammetry (LSV) at a scan rate of 5 mV s^{-1}. Unless otherwise specified, all LSV curves were corrected with 95% iR compensation. The electrochemical double layer capacitance (Cdl) was determined from CV measurements performed in the non-faradaic potential region. CV experiments were carried out at multiple scan rates (20, 40, 60, 80, and 100 mV s^{-1}) within a potential window of 0.0 to 0.1 V versus RHE. The current density difference (Δj) at the midpoint potential of 0.05 V was measured. Cdl was subsequently calculated from the slope of the linear relationship between Δj and the scan rate, with the slope taken as a measure of the capacitive current. Subsequently, the Cdl values derived from the aforementioned method were employed to determine the electrochemical active surface area (ECSA) of the catalyst. Electrochemical impedance spectroscopy (EIS) measurements were performed over a frequency range of 100 kHz to 0.01 Hz at potentials specific to each material, which corresponded to the overpotentials obtained at a current density of 10 mA cm^{-2} via linear sweep voltammetry (LSV), using an AC amplitude of 5 mV. The cycling stability test was conducted as follows: prior to the main measurement, the carbon cloth electrode loaded with ZrP/Pt was subjected to approximately 20 CV cycles within a potential range of 0 to -0.5 V versus RHE in 1 M KOH, using a scan rate of 100 mV s^{-1}. After the current response stabilized, the electrode was removed from the electrochemical cell and allowed to rest for approximately 10 minutes to minimize residual charge effects before further testing. Subsequently, LSV was conducted at a scan rate of 5 mV s^{-1} to obtain the pre-cycling polarization curve. Thereafter, the electrode underwent a CV stability test in 1 M PBS with a potential window of 0 to -0.5 V (vs. RHE), using a scan rate of 100 mV s^{-1} for 5000 cycles. Following the stability test, the electrode was allowed to equilibrate for 10 minutes prior to acquiring the post-cycling LSV measurement.

Calculation of turnover frequency (TOF) values

The TOF is calculated by the following equations [2, 3]:

$$TOF = \frac{Total\ hydrogen\ turnovers\ per\ geometric\ surface\ area}{Active\ sites\ per\ geometric\ surface\ area}$$

The total number of hydrogen turnover events was determined based on the current density by applying the following formula:

$$Total\ hydrogen\ turnovers = \left[|j|\left(mA\ cm^{-2}\right)\right]\left[\frac{1(Cs^{-1})}{10^3(mA)}\right]\left[\frac{1\left(mol\ e^{-1}\right)}{96485(C)}\right]\left[\frac{1\ mol\ H_2}{2\ mol\ e^{-1}}\right]\left[\frac{6.02\times10^{23}\ molecules\ H_2}{1\ mol\ H_2}\right]$$

$$= 3.12\times10^{15}|j|H_2\ s^{-1}cm^{-2}per\ mA\ cm^{-2}$$

$$\text{Active sites per geometric surface area (noble metal)} = \left[\frac{Catalyst\ loading\ on\ the\ electrode\ \left(g\ cm^{-2}\right)\times\ noble\ metal\ content(wt\%)}{noble\ metal\ atomic\ weight\ \left(g\ mol^{-1}\right)}\right]\times 6.02\times10^{23}\ site\ mol^{-1}$$

$$TOF = \frac{3.12 \times 10^{15}}{Number\ of\ active\ sites} \times |j|$$

The TOF values reported in this study were calculated under the assumption that all Pt atoms in the catalyst, rather than solely the surface-exposed Pt atoms, are accessible for the hydrogen evolution reaction.

DFT Calculations

The density functional theory (DFT) calculations were carried out with the VASP code.[4] The Perdew–Burke–Ernzerhof (PBE) functional within generalized gradient approximation (GGA)[5] was used to process the exchange–correlation, while the project or augmented-wave pseudopotential (PAW)[6] was applied with a kinetic energy cut-off of 500 eV, which was utilized to describe the expansion of the electronic eigenfunctions. The vacuum thickness was set to be 15 Å to minimize interlayer interactions. The Brillouin-zone integration was sampled by a Γ-centered 5 × 5 × 1 Monkhorst–Pack k-point. All atomic positions were fully relaxed until energy and force reached a tolerance of 1×10^{-6} eV and 0.01 eV/Å, respectively. The dispersion corrected DFT-D method was employed to consider the long-range interactions.[7] Employing the climbing image nudged elastic band method (CI-NEB), we computed the minimum energy pathway of the reaction along with its corresponding activation barrier.

The Gibbs free energy change (ΔG) was calculated by computational hydrogen electrode (CHE) model as follows:

$\Delta G = \Delta E + \Delta ZPE - T\Delta S$

where ΔE is the reaction energy obtained by the total energy difference between the reactant and product molecules absorbed on the catalyst surface and ΔS is the change in entropy for each reaction, ΔZPE is the zero-point energy correction to the Gibbs free energy.

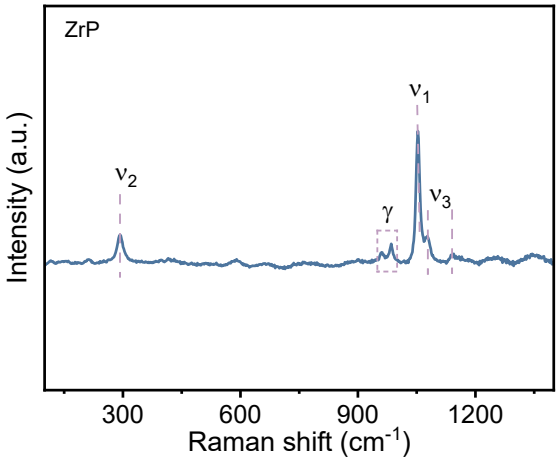

Figure S1. The Raman spectra of ZrP.

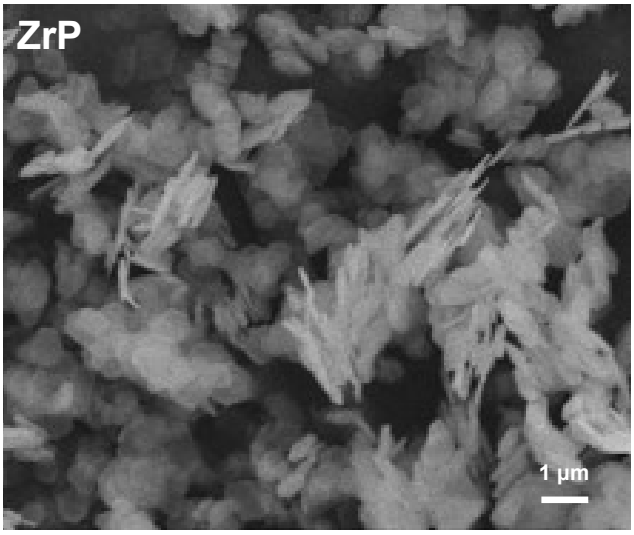

Figure S2. SEM images of ZrP.

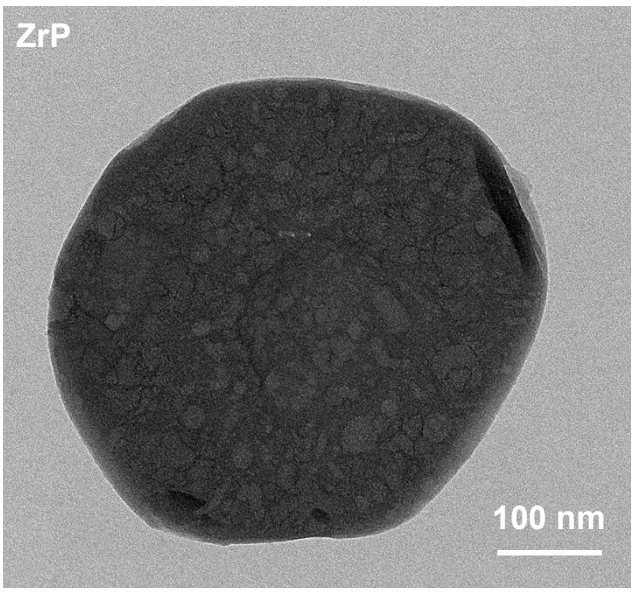

Figure S3. TEM images of ZrP.

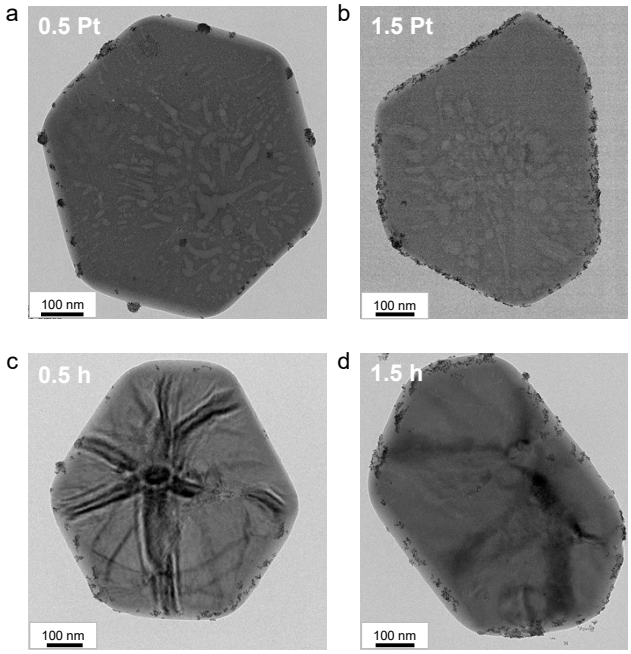

Figure S4. TEM images of (a) ZrP/0.5Pt, (b) ZrP/1.5Pt, (c) ZrP/Pt-0.5 h and (d) ZrP/Pt-1.5 h

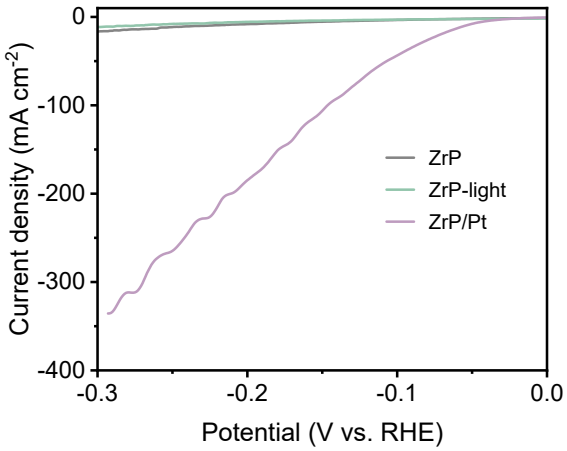

Figure S5. HER LSV curves of ZrP-light, ZrP and ZrP/Pt.

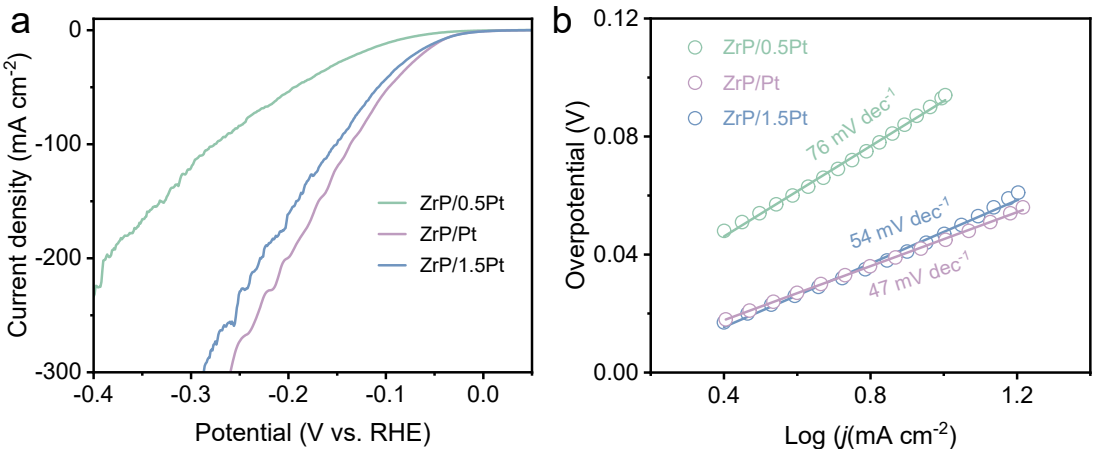

Figure. S6. The HER performance of catalysts with different Pt loading amounts in 1 M KOH.

(a) HER LSV curves and (b) Tafel slope of ZrP/0.5Pt, ZrP/Pt and ZrP/1.5Pt.

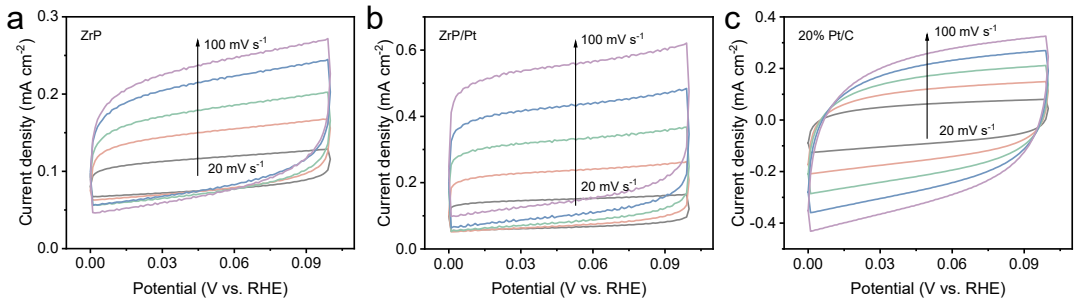

Figure S7. CV curves recorded in non-faradaic regions at various scan rates.

(a) ZrP, (b) ZrP/Pt and (c) 20% Pt/C.

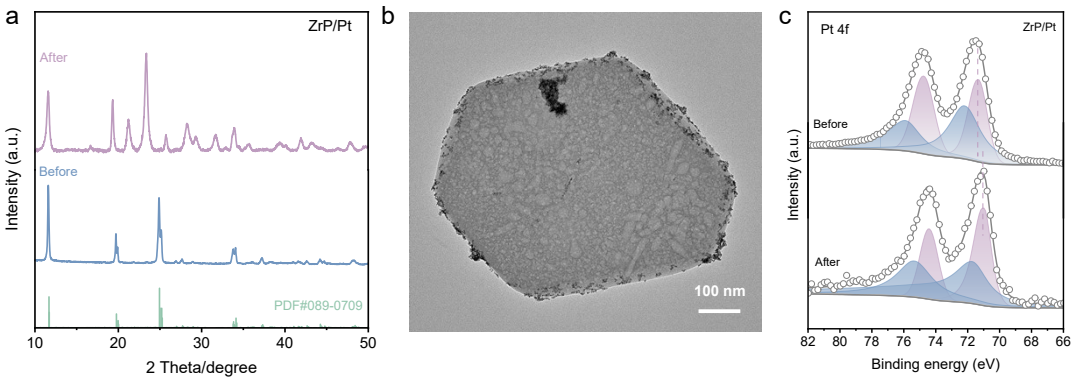

Figure S8. The morphology characterizations after stability tests indicate that the morphology and structure of ZrP/Pt have remained largely unchanged.

(a) The XRD patterns of ZrP/Pt before and after stability tests. (b) TEM images of ZrP/Pt after stability tests. (c) Pt 4f XPS spectra for the ZrP/Pt before and after.

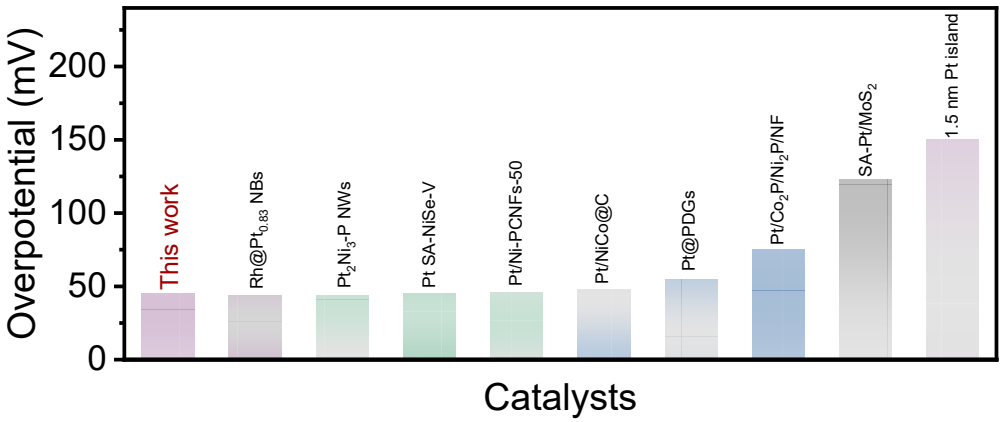

Figure S9. Comparison of the alkaline HER performance for ZrP/Pt catalyst with other Pt-based catalysts

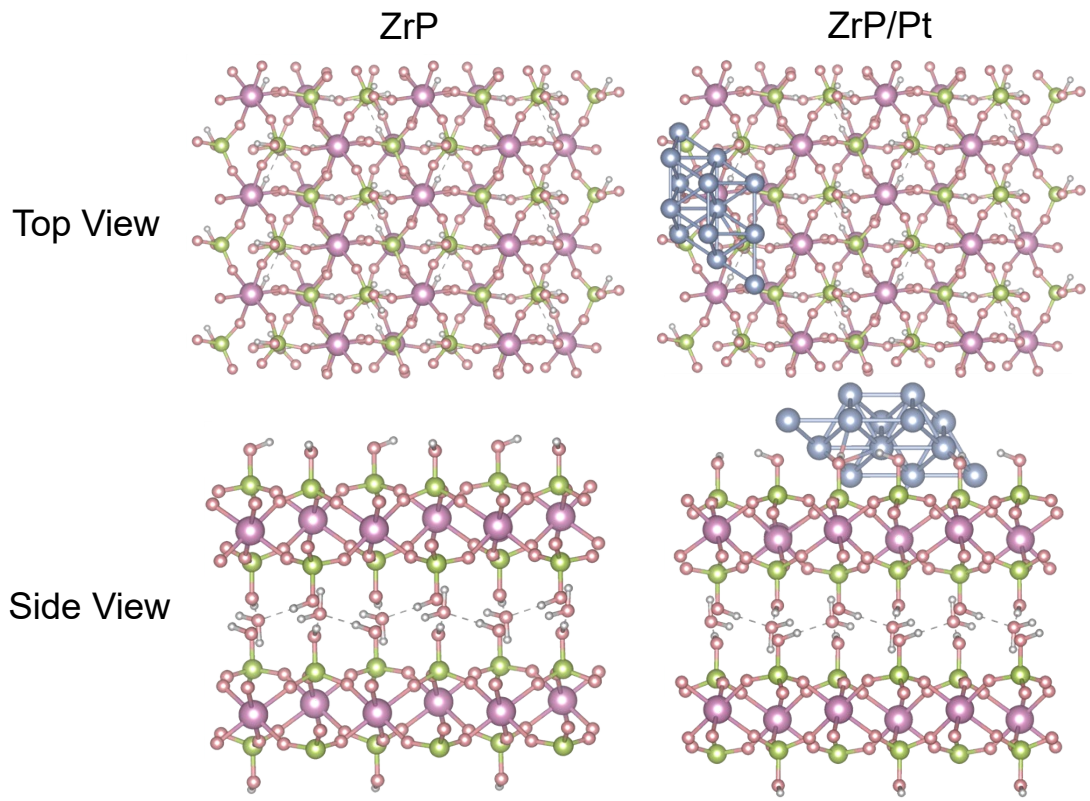

Figure S10. The top and side view of the atomic structure of different samples

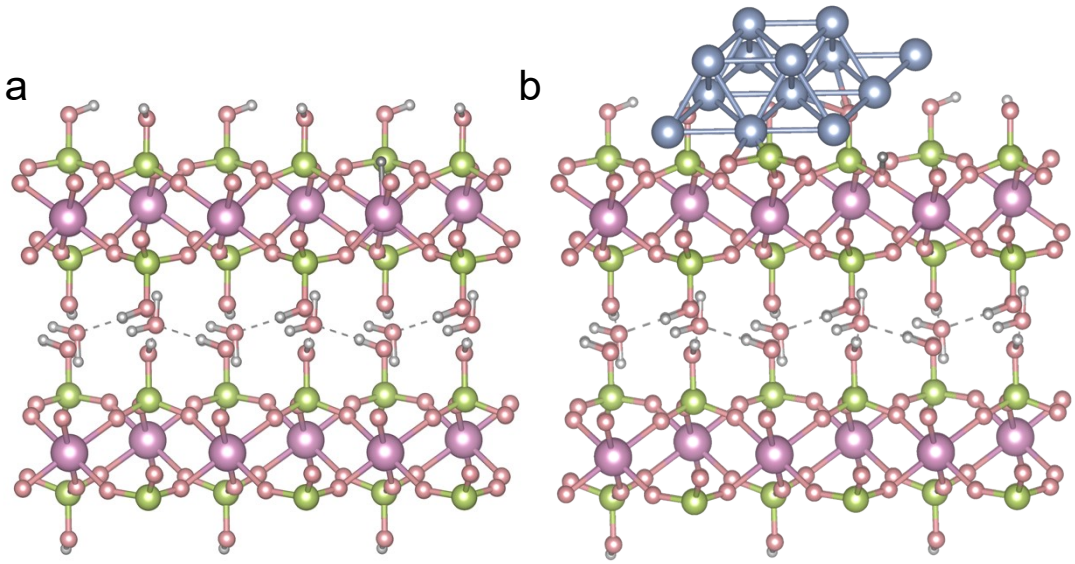

Figure S11. Optimized atomic structure of H adsorption on (a) ZrP and (b) ZrP/Pt.

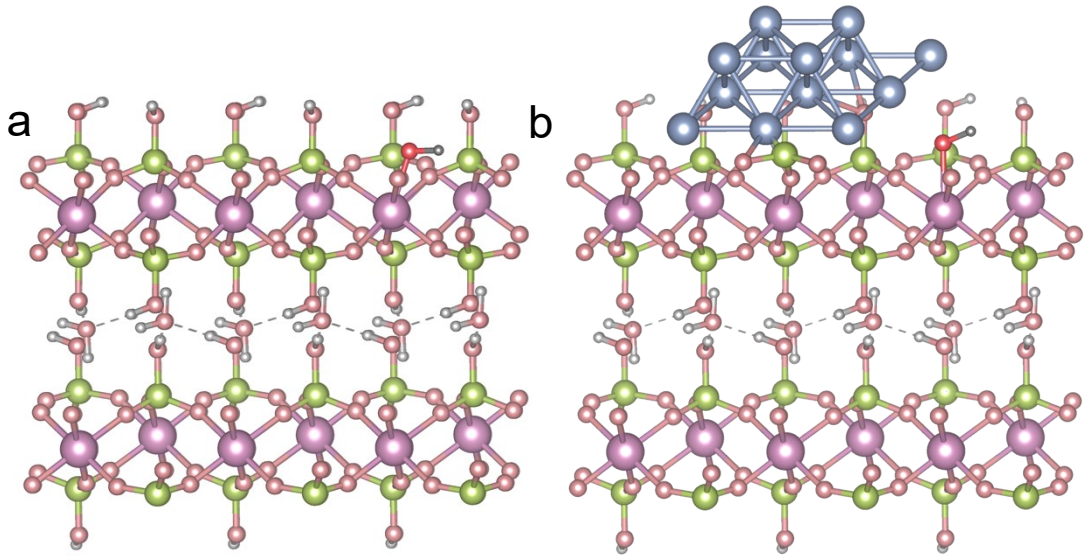

Figure S12. Optimized atomic structure of OH adsorption on (a) ZrP and (b) ZrP/Pt.

Table S1. The ICP-OES analysis of ZrP/Pt.

Catalyst	Element	Wt. %
ZrP/Pt	Pt	1.66%

Table S2. Comparison of the alkaline HER performance for ZrP/Pt catalyst with other catalysts

Catalysts	η_{10} (mV)	Tafel slope (mV dec^{-1})	Mass activity (A mg^{-1})	Reference
ZrP/Pt	45	43	10.26@--0.1V	This work
Pt SA-NiSe-V	45	52	1.59@-0.1V	*Angew. Chem. Int. Edit.* ***2023****, 62, e202308686*
Pt/Ni-PCNFs-50	46	43.8	2.22@ -0.1V	*Chin. Chem. Lett.* ***2023****, 34, 107359-107359*
Pt/NiCo@C	48	134	-	*Electrochim. Acta.* ***2023****, 460, 142634-142642*
1.5 nm Pt island	150	43	-	*Chem. Mater.* ***2023****, 35, 8636-8644*
Rh@$Pt_{0.83}$ NBs	44	54.2	2.36@-0.07 V	*Chem. Eng. J.*, **2022**, 429, 132414
SA-Pt/MoS_2	123	76.7	-	*Small.* ***2021****, 18, 2104824-2104834*
Pt@PDGs	55	79.2	-	*New J. Chem.*, **2021**,45, 21670-21675
Pt_2Ni_3-P NWs	44	46	-	*Chem. Mater.* ***2020****, 32, 3144-3149*
Pt/Co_2P/Ni_2P/NF	75	64	-	*Sustainable Energy Fuels.* ***2020****, 5, 1059-106*

References

1. R. Wang, Y. Li, X. Tan, J. Zhang, C. Li, L. Cao and B. Dong, *Advanced Materials Interfaces*, 2022, **9**, 2200387.
2. D. Liu, X. Li, S. Chen, H. Yan, C. Wang, C. Wu, Y. A. Haleem, S. Duan, J. Lu, B. Ge, P. M. Ajayan, Y. Luo, J. Jiang and L. Song, *Nature Energy*, 2019, **4**, 512-518.
3. G. Feng, F. Ning, J. Song, H. Shang, K. Zhang, Z. Ding, P. Gao, W. Chu and D. Xia, *Journal of the American Chemical Society*, 2021, **143**, 17117-17127.
4. G. Kresse and J. Furthmüller, *Computational Materials Science*, 1996, **6**, 15-50.
5. J. P. Perdew, K. Burke and M. Ernzerhof, *Physical Review Letters*, 1996, **77**, 3865-3868.
6. P. E. Blöchl, *Physical Review B*, 1994, **50**, 17953-17979.
7. S. Grimme, *Journal of Computational Chemistry*, 2006, **27**, 1787-1799.